Journal of Bone and Mineral Metabolism (2019) 37:385–398
https://doi.org/10.1007/s00774-018-0936-x

ORIGINAL ARTICLE

Biodistribution of strontium and barium in the developing and mature skeleton of rats

Arash Panahifar[1] · L. Dean Chapman[1,2] · Lynn Weber[3] · Nazanin Samadi[4] · David M. L. Cooper[1]

Received: 14 March 2018 / Accepted: 7 May 2018 / Published online: 19 June 2018

Abstract

Bone acts as a reservoir for many trace elements. Understanding the extent and pattern of elemental accumulation in the skeleton is important from diagnostic, therapeutic, and toxicological perspectives. Some elements are simply adsorbed to bone surfaces by electric force and are buried under bone mineral, while others can replace calcium atoms in the hydroxyapatite structure. In this article, we investigated the extent and pattern of skeletal uptake of barium and strontium in two different age groups, growing, and skeletally mature, in healthy rats. Animals were dosed orally for 4 weeks with either strontium chloride or barium chloride or combined. The distribution of trace elements was imaged in 3D using synchrotron K-edge subtraction micro-CT at 13.5 µm resolution and 2D electron probe microanalysis (EPMA). Bulk concentration of the elements in serum and bone (tibiae) was also measured by mass spectrometry to study the extent of uptake. Toxicological evaluation did not show any cardiotoxicity or nephrotoxicity. Both elements were primarily deposited in the areas of active bone turnover such as growth plates and trabecular bone. Barium and strontium concentration in the bones of juvenile rats was 2.3 times higher, while serum levels were 1.4 and 1.5 times lower than adults. In all treatment and age groups, strontium was preferred to barium even though equal molar concentrations were dosed. This study displayed spatial co-localization of barium and strontium in bone for the first time. Barium and strontium can be used as surrogates for calcium to study the pathological changes in animal models of bone disease and to study the effects of pharmaceutical compounds on bone micro-architecture and bone remodeling in high spatial sensitivity and precision.

Graphical abstract

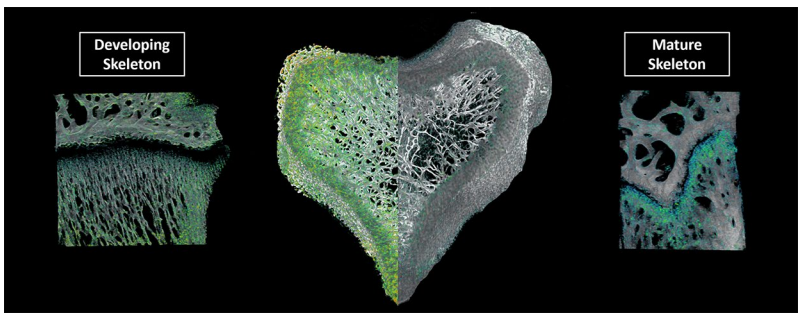

Keywords Bone · Synchrotron · Barium · Strontium · K-edge subtraction imaging

Electronic supplementary material The online version of this article (https://doi.org/10.1007/s00774-018-0936-x) contains supplementary material, which is available to authorized users.

✉ Arash Panahifar
a.panahifar@usask.ca

Extended author information available on the last page of the article

Abbreviations

3D	3-Dimensional
ANOVA	Analysis of variance
BMIT	Biomedical imaging and therapy
CLS	Canadian light source
ECG	Electrocardiogram
ELISA	Enzyme-linked immunosorbent assay

EPMA	Electron probe micro analysis
GLM	General linear model
ICP-MS	Inductively coupled plasma mass spectrometry
ICP-OES	Inductively coupled plasma optical emission spectrometry
KES	K-edge subtraction
Micro-CT	Micro-computed tomography
PET	Positron emission tomography
SPECT	Single-photon-emission computed tomography
XRF	X-ray fluorescence imaging

Introduction

Distribution of trace elements in the body and their accumulation into skeleton has been documented for a long time. With the introduction of new technologies, the ability to not only detect and quantify the presence, but also to visualize the location of the elements becomes feasible. Elements from various groups are known to accumulate in bone [1–3]; however, those from group 2, the alkali earth metals, are of particular interest because of their strong affinity for bone. Calcium, the most abundant inorganic element in bone's hydroxyapatite crystalline matrix, belongs to this group. Due to the similarity in the chemical and physical properties such as electric charge and ionic radius, many elements in alkali earth metals group can incorporate into bone through adsorption to the surface or by replacing calcium atoms in the hydroxyapatite structure [4–6]. This is significant from diagnostic, therapeutic, and even toxicological perspectives. For example, if one element is incorporated in the structure of hydroxyapatite, instead of weak adsorption to the surface, then the long-term effects of that element on bone cells become important as well as radiation decay pattern and half-life if the element is radioactive. Radioactive forms of bone-seeking elements (e.g., ^{18}fluorine, ^{89}strontium) have been used for palliative treatment [7, 8] or diagnosis of cancers affecting musculoskeletal system. None-radioactive forms of some elements such as strontium [9, 10], and more recently lanthanum [11, 12], have been suggested for treatment of musculoskeletal diseases such as osteoporosis. Though, possible overestimation of benefits for osteoporosis, measured by X-ray absorptiometry, must be considered due to larger attenuation of photons by these heavier elements [13].

Incorporation of strontium and barium in bone and more specifically in the hydroxyapatite structure has been studied by our group and others [5, 14–16]. Spatial distribution of elements can be imaged by 2-dimensional (2D) methods such as autoradiography (if radioactive) [6], Electron Probe Micro Analysis (EPMA) [17, 18], and X-ray fluorescence imaging (XRF) [1], or 3-dimensional (3D) methods such as dual energy K-edge subtraction (KES) micro-computed tomography (micro-CT), which is employed in this study [[19]14–16]. Although gamma rays from single-photon-emission computed tomography (SPECT) and positron-emission tomography (PET) can also be reconstructed to 3D images, due to their low resolution, they are not discussed in this article. Radioisotopes of strontium have been used in clinics for a long time, while stable forms as calcium surrogates have only recently been proposed to be of diagnostic value in preclinical animal models or biopsies from humans [14]. We have further looked at the possibility of using stable barium as a bone turnover tracer using KES [15] and spectral KES [20] methods that are suitable for ex vivo and in vivo applications, respectively. The sample dimensions for imaging are dictated by its X-ray linear attenuation coefficient, which is dependent on scanning X-ray energy. Diagnostic use of strontium as a 3D tracer is mostly suited for investigating small sample biopsies due to its low K-edge energy (16.105 keV) that consequently limits the sample dimensions to 2–3 mm thickness of bone (strontium contribution not included). On the other hand, barium is only present in the body in minute amounts, is from the same group, and has a K-edge energy of 37.441 keV which enables assessment of much larger samples (20–25 mm bone thickness; barium contribution not included). In fact, if barium and strontium co-localize in the same area and are not associated with major adverse effects, then barium could be considered as a bone tracer, at least in preclinical studies.

Barium in its soluble form, which is the bioavailable form, is highly toxic. The main toxicities of barium are associated with the cardiovascular system as it acts as a potassium channel blocker; hence, it will cause cardiac arrest if sufficient concentration is consumed [21]. The toxic effects of barium on heart can be measured from the electrocardiogram (ECG) as the cardiotoxicity is manifested by prolongation of the *Q–T* interval. However, in low doses, barium has been indicated as safe [22, 23]. In our previous studies with low-dose administration of barium for 4 weeks, we did not observe any obvious side effects [15]. On the other hand, strontium is not a potassium channel blocker and in some countries is available either as prescription or an over-the-counter supplement for increasing bone mineral density via a suggested dual effect mechanism of simultaneously reducing bone resorption and promoting bone formation, though its mechanism and effectiveness is still subject to debate [24, 25]. Recently, concerns were raised about the increased risks of cardiovascular disease in patients who received long-term strontium ranelate, concerns that may lead to discontinuation of the drug for osteoporosis treatment [26]. In the current study, only low doses of strontium and barium chloride were used, for a short period of time. Moreover, we collected electrocardiogram and blood sample for in-depth toxicological

assessment. This article focuses on comparing the nature, extent, and pattern of the accumulation of barium and strontium in the skeleton of healthy rats from juvenile and adult age groups. We hypothesize that barium and strontium will co-localize in the same regions, primarily in the newly forming sites. If barium, at a safe dose, can target areas of bone remodeling, it can be employed as a tracer for investigating role of remodeling in the preclinical models of bone disease, and subsequently for evaluating drug effectiveness in those conditions. Beyond archaeological studies [27, 28], there are very few articles that compare the pattern and extent of incorporation of alkali earth metals in the bone. To the best of our knowledge, this article is the first to compare the spatial distribution of strontium and barium in the skeleton.

Materials and methods

Materials

Barium chloride dihydrate ($BaCl_2{\cdot}2H_2O$, $\geq 99\%$ purity, MW 244.26 g/mol) and strontium chloride hexahydrate ($SrCl_2{\cdot}6H_2O$, 99% purity, MW 266.62 g/mol) were purchased from Sigma-Aldrich (Oakville, ON, Canada). Urea (DIUR-500) assay kit was purchased from BioAssay Systems.

Animals

36 healthy Sprague–Dawley male rats of two different age groups of 1-month old (i.e., developing skeleton) or 8-month old (i.e, mature skeleton) were randomly divided into 8 groups (Table 1).

Upon arrival, rats were acclimatized for 1 week. Two rats were housed in each cage.

Weights of animals were recorded weekly. Barium chloride and/or strontium chloride were dissolved in distilled water and dosed to animals orally with a curved feeding needle at equal molar concentrations for 28 days. Barium dosage was 58.5 mg/kg/day (equivalent to 33 mg/kg/day free Ba^{2+}) and strontium dosage was 64.75 mg/kg/day (equivalent to 21.3 mg/kg/day free Sr^{2+}), while the co-dosed groups received both strontium and barium. The dosage was selected based on our previous work to achieve detectable elemental levels in bone without toxic adverse effects [15, 20]. Control animals received the same volume (1 mL/kg) of distilled water. Animals were fasted 2 h before and after the administration to minimize competitive uptake of dietary calcium by bone. Animals received sweetened dry breakfast cereal as treat after each treatment. After 28 days of treatment, rats were euthanized by exsanguination while under isoflurane anesthesia. Blood samples were collected at the baseline and at the time of euthanasia. Hind limbs were dissected free of soft tissues and were frozen for later KES imaging. The animal use protocol (# 20110124) was approved by the University of Saskatchewan Animal Research Ethics Board.

Synchrotron K-edge subtraction imaging

The 3D distribution of barium and strontium in bones was imaged using high-resolution synchrotron KES-micro-CT imaging at the Biomedical imaging and therapy (BMIT)-bending magnet beamline [29] of the Canadian light source (CLS). The full details on this methodology are reported in our previous published works [14–16]. Briefly, bones were air-dried in an oven at 45 °C for 24 h. This is necessary as evaporation of moisture in samples during imaging complicates image analysis. Tibial and femoral epiphyses were transversely cut from their metaphyses for mounting on the sample holder with superglue. Barium-dosed bones were scanned as whole epiphyses, while strontium-dosed samples were cut in smaller pieces (approximately 2–3 mm solid bone thickness) to avoid photon starvation artifacts at the low energy K-edge of strontium [14].

The K-edge of strontium and barium occurs at 16.105 and 37.441 keV, respectively. Samples were scanned slightly above (E_{Above}) and below (E_{Below}) the K-edge energies, followed by the subtraction of the two data sets, specifically, 37.441 ± 0.060 keV for barium and 16.105 ± 0.050 keV for strontium. These energy gaps were determined by observing complete 'edge-crossing', while phantoms were in the beam pathway. The scans consisted of 1125 projections collected at each energy through 180° rotation in step and

Table 1 Experimental groups

Group	Barium old (BAO)	Co-dosed old (BSO)	Strontium old (SRO)	Control old (CONO)	Barium young (BAY)	Co-dosed young (BSY)	Strontium young (SRY)	Control young (CONY)
Age	Adult (8-month old)				Juvenile (1-month old)			
Treatment	Barium	Barium and Strontium	Strontium	Water	Barium	Barium and strontium	Strontium	Water
Number of animals	6	6	6	3	6	6	6	3

shoot mode with 0.16° angular step. A Hamamatsu ORCA-Flash 4.0 detector at 13.5 µm pixel size coupled with an AA60 scintillator [10 µm, P43 (Gd_2O_2S:Tb)] was used. The sides of camera were covered with a lead shielding to reduce response from scattered X-rays and cooled with water to further reduce electronic noise. 'Before' and 'after' each scan, 10 projections were acquired with no object in the path (i.e., bright field images), as well as 10 projections with no X-rays (i.e., dark field images), to perform image normalization. The synchrotron ring flux decay was also corrected with flat 'before' and 'after' projections using the ANKAphase software [30]. A 0.5 mm aluminum filter was placed before the monochromator for imaging at the strontium energies and a 1.1 mm aluminum filter for imaging at the barium energies to reduce power loading on the monochromator. Exposure time was automatically set at maximum photon count for each scan using the detector software and kept constant during the scan. Exposure times ranged from 3 to 4 s/projection and 1–1.5 s/projection for barium and strontium energies, respectively. Reconstruction of the data was performed using the Nrecon software v.1.6.10.2 (Bruker micro-CT, Belgium). Amira v.6.0.0 (FEI, France) was used to visualize the data set, and for 3D registration and subtraction of the CT data sets. Since KES is a quantitative imaging method, the spatial concentration of elements of interest was obtained.

Electron probe microanalysis (EMPA)

To validate the results from the KES-micro-CT, same samples were scanned with EPMA (Cameca SX100, Cedex, France). Samples were immersed in 95% ethanol for 2 weeks, followed by 1 week immersion in acetone and 2 days in an oven at 45 °C. Subsequently, the samples were embedded in epoxy (EpoThin, Buehler Ltd.) and surface-polished for mapping. The mapping parameters were: pixel size = 5 µm or 7 µm, exposure time = 15 ms, current = 30 nA. The maps of following elements were acquired: strontium, barium, calcium, phosphorus, magnesium.

Toxicological evaluation

To investigate the possible adverse effects of barium on the cardiovascular system (e.g., Q–T interval prolongation), rats were anesthetized with isoflurane and ECG was collected at 1 day after the termination of the dosing period. The cardiotoxicity of barium is known to be caused by blocking K^+ channels [21]; however, strontium is not known to block K^+ channels. Due to technical issues, ECG was not collected from control groups, and strontium-treated rats were considered as controls for the purpose of ECG experiment.

To assess the toxicity of barium and strontium administration on kidneys, blood urea levels were measured by ELISA assay (enzyme-linked immunosorbent assay). The procedure was followed according to manufacturer's protocol and tests were run in duplicates. Serum was separated by centrifuging blood samples at 4000 rpm and 4 °C for 20 min and stored at − 20 °C.

Mass spectrometry

Three whole tibiae from each group were dried in an oven at 45 °C and were powdered using a previously cleaned mortar and pestle. Powdered samples were weighed and submitted for inductively coupled plasma mass spectrometry (ICP-MS) to determine elemental content. Moreover, serum samples from 3 animals of each group were submitted for mass spectrometry using inductively coupled plasma optical emission spectrometry (ICP-OES). To control the quality of the daily dosing solutions, aliquots were analyzed using ICP-OES.

Statistical analysis

Statistical analyses were performed by the IBM SPSS Statistics software (version 24). Univariate General Linear Model (GLM), *t* test, and Pearson's correlation tests were used in this study. The type of test used for each experiment is explained in the results section. Statistical significance was $p < 0.05$. Shapiro–Wilk test was used for test of normality and Tukey's test was used for post hoc analysis.

Results

All animals tolerated the treatments well, and no apparent signs of toxicity were observed. All animals gained weight at a similar rate during the study (Supplemental Information). Barium and strontium were primarily incorporated in the areas of active bone formation during the treatment. Those areas were limited to occasional bone remodeling in trabecular and cortical bone in the adult rats, whereas in the juveniles, significantly higher concentrations were incorporated in both trabecular and cortical bones and in broader regions. Barium and strontium deposits were found in the growth plates of older rats, because growth plates never close completely in rats; however, the concentration of the elements was significantly lower compared to juvenile animals that were quickly growing at the time of administration. Although quantitative analysis of maximum concentration per pixel was not carried out, qualitative examination of the concentration scale bars shows that maximum concentration of each trace element is within a similar range regardless of age, but the number of active bone formation regions is much less prevalent in the older rats (Fig. 1).

As hypothesized, barium and strontium co-localized in the same regions (Figs. 2, 3, 5, 6). The BSY (co-dosed

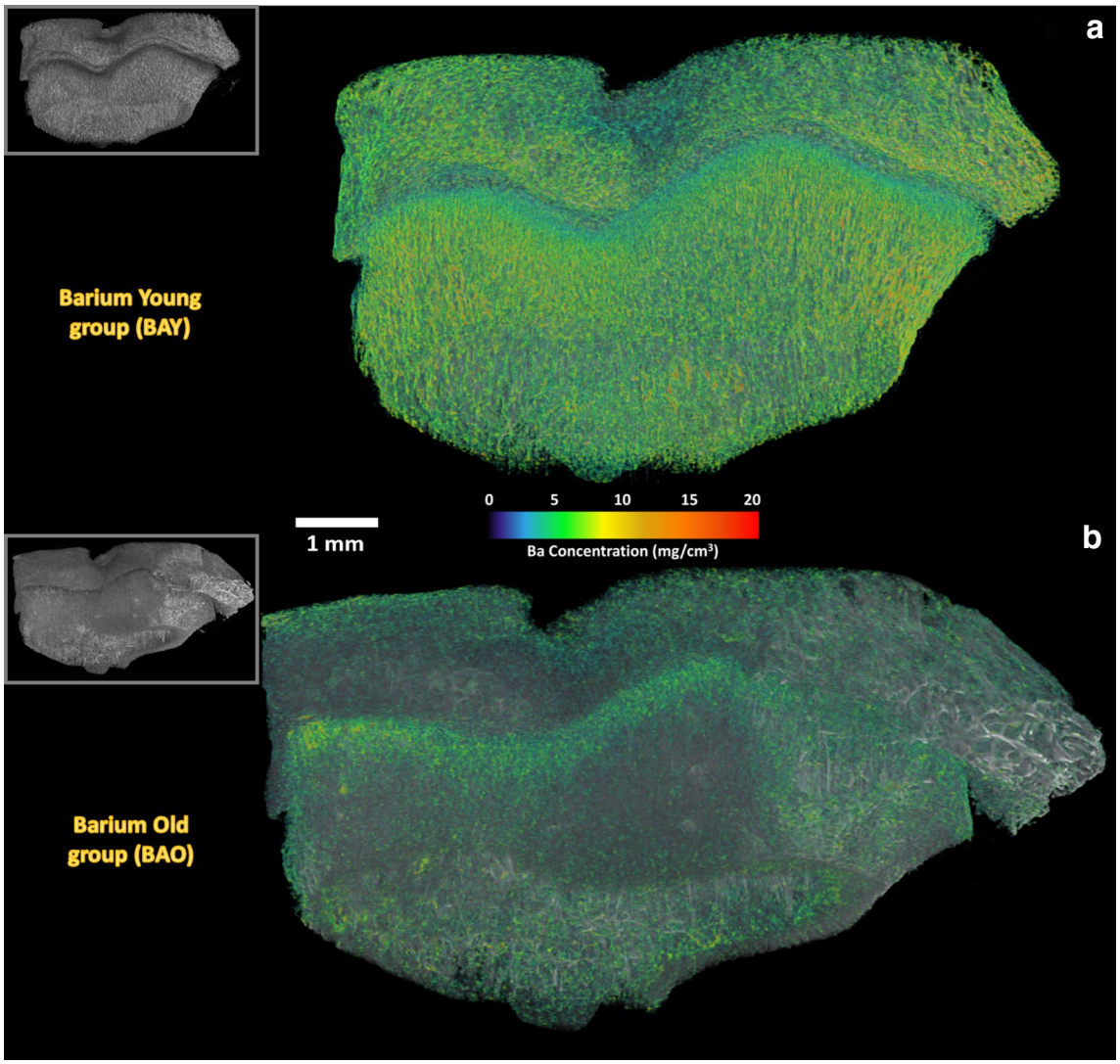

Fig. 1 3D KES images of barium distribution. **a** Accumulation of barium in the tibia of a juvenile rat. **b** Distribution of barium in the tibia of an adult rat. Bones are rendered in grey and barium concentration is represented in colour on top of the grey render. Note that the barium concentration range per pixel is similar; however, bone forming regions are more prevalent in the juvenile rat. The insets show the plain 3D models of the respective bones for the sole purpose of anatomical reference

young) and BSO (co-dosed old) groups received equal molarity of both strontium and barium. The KES scans of these samples were collected around the K-edge energies of both elements. The subtle differences in their spatial location are due to noise and relatively thick samples for strontium K-edge imaging that completely attenuates some of the low energy X-rays within the sample. This is avoidable by collecting longer scans and thinner samples. The difference between the concentrations is explained in "Discussion".

Barium and strontium were only present in minute concentrations in the bones of control animals [Figs. 4, 5, CONO (control old) group]. Concentrations in some samples were below the detection limit of ICP-MS, whereas the KES showed some faint signal that could be attributed to noise and misregistration of the 'above' and 'below' images.

EPMA images have relatively better signal-to-noise ratio, are not affected by the thickness of sample for barium and strontium mapping (i.e., EPMA is a surface method), and misregistering of images are not applicable. EPMA data (Figs. 5, 6) confirm that the same pattern of incorporation observed in the KES 3D images.

Juvenile animals had incorporated more strontium and barium than the adults, despite having lower concentrations of these elements in their serum (Table 2; Fig. 7). The effect of age on barium and strontium uptake was tested with a *t* test between pooled young and old groups. Young rats receiving strontium had incorporated 2.3-fold

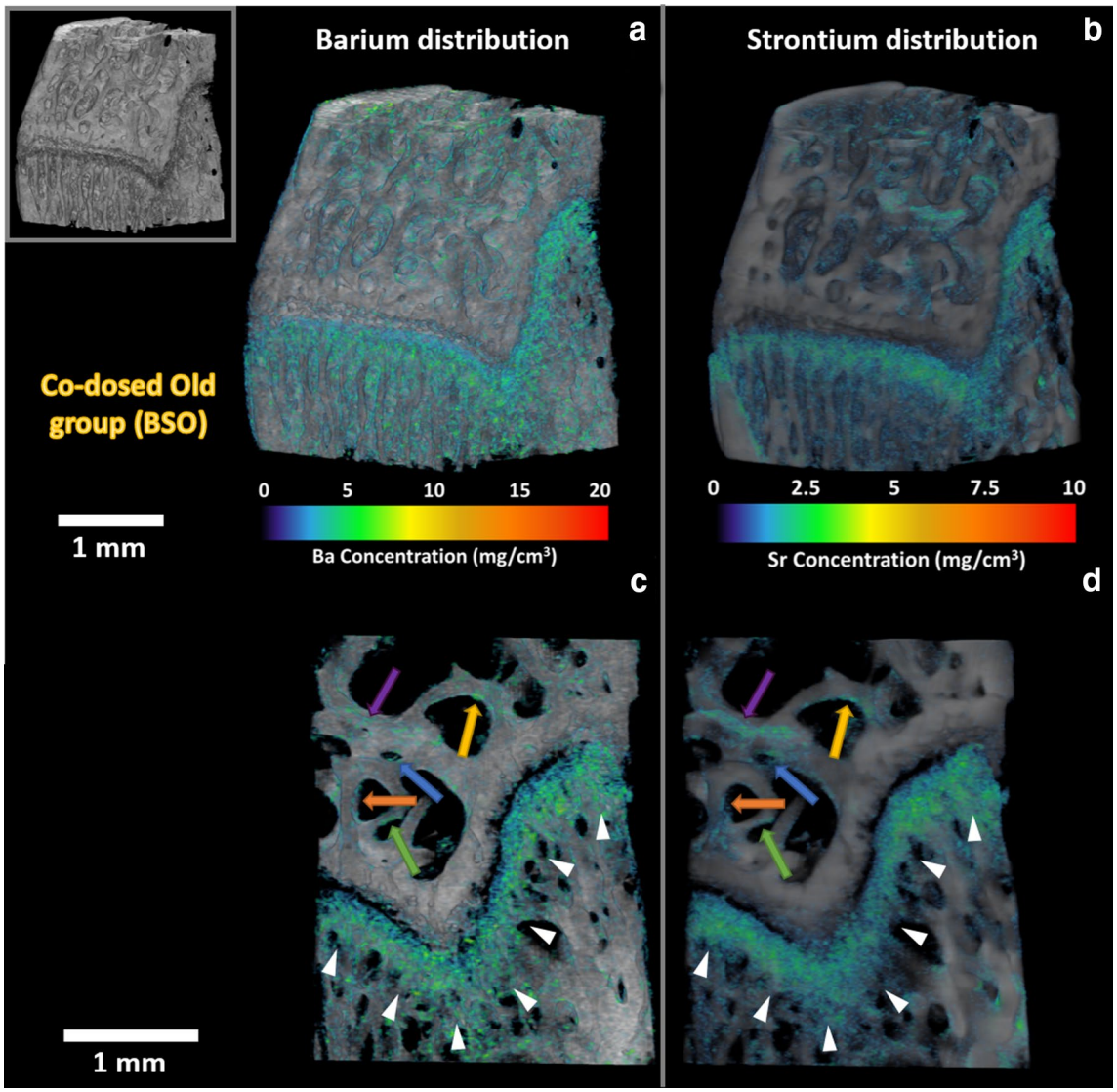

Fig. 2 Co-localization of barium and strontium in adult rats. **a**, **c** Barium distribution in the tibia of a co-dosed adult animal. **b**, **d** Strontium distribution in the same sample. The bottom panels are a stack of 20 CT slices for better visualization of finer details. Bones are rendered in grey and barium concentration is represented in colour on top of the grey render. The colored arrows indicate co-localization of barium and strontium in the same regions. The white arrowheads indicate accumulation of barium and strontium in the growth plate. The inset shows a plain 3D model of the respective bone

more strontium in their bone than old rats ($p = 0.003$), whereas serum levels of strontium were 1.5 times less in juveniles ($p = 0.042$). Similarly, young rats receiving barium had incorporated 2.3-fold more barium than old rats in their bone ($p = 0.0005$). Serum levels of barium were also lower in juvenile rats, however, that difference was not statistically significant ($p = 0.066$), likely due to small sample number. Co-administration did not have any effect on the amount of barium or strontium intake by bone, compared to singly dosed groups.

There was no statistical difference in the serum levels of strontium among the treatment groups that received strontium (either solely or in combination with barium). The same was true for the barium treated groups. Univariate analysis of variance with Tukey's post hoc analysis was used for between groups comparison. BSY group incorporated 2.7 times more strontium ($p = 0.023$) and 2.1 times more barium ($p = 0.007$) in bone compared to BSO group. In addition, it incorporated 2.4-folds more strontium than SRO (strontium old) ($p = 0.035$) and 3.0-fold more barium than BAO (barium old) ($p = 0.001$) groups. BAY (barium young) group

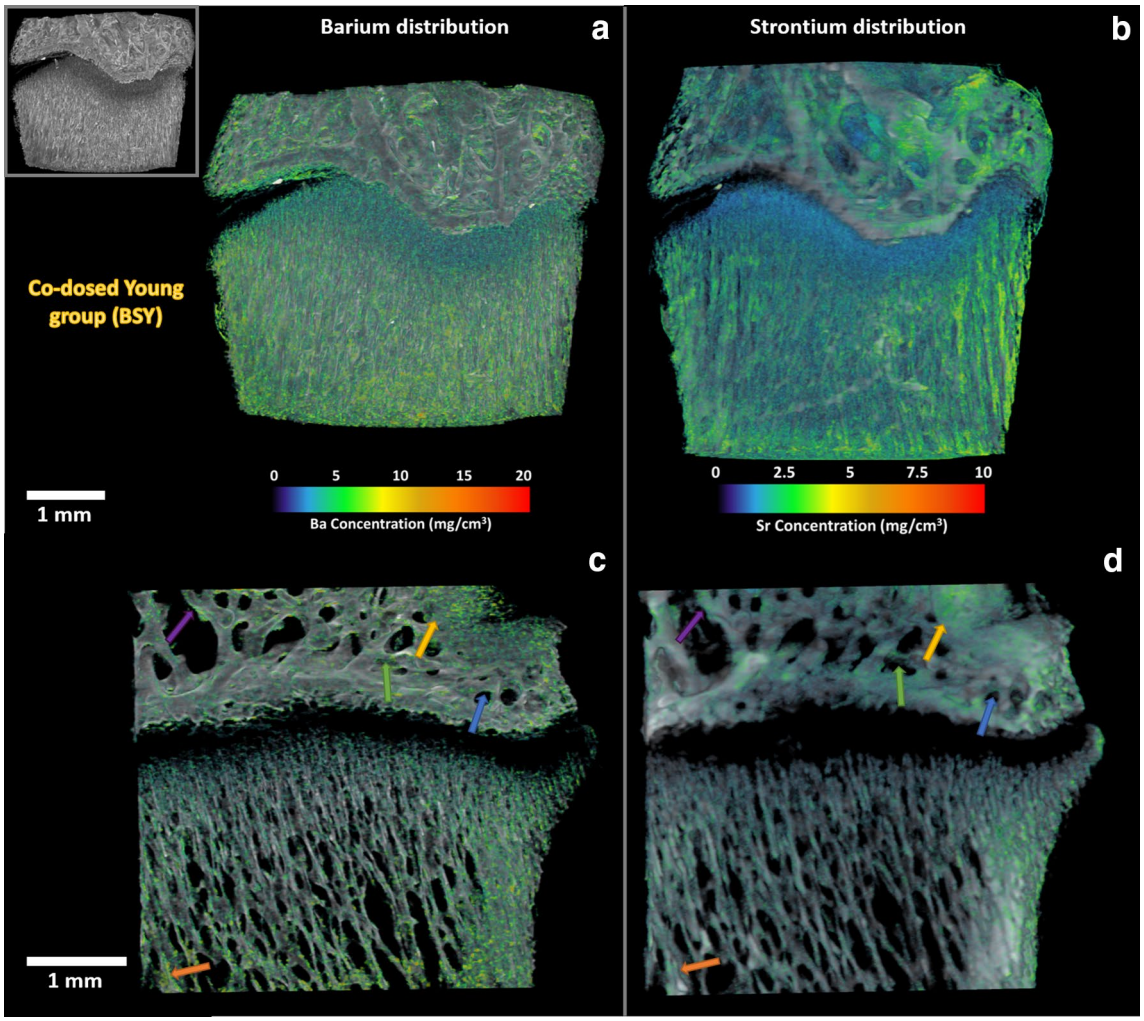

Fig. 3 Co-localization of barium and strontium in juvenile rats. **a**, **c** Barium distribution in the tibia of a co-dosed juvenile animal. **b**, **d** Strontium distribution in the same sample. The bottom panels are a stack of 20 CT slices for better visualization of finer details. The colored arrows indicate co-localization of barium and strontium in the same regions. Note the significantly higher number of calcification and remodeling events compared to older animals (Fig. 2). The inset shows a plain 3D model of the respective bone

incorporated 2.6-fold more barium in bone than BAO group ($p = 0.006$) and 1.8-folds more than BSO ($p = 0.033$). The similar pattern was witnessed for SRY (strontium young) group, though it was not statistically significant, likely due to the small sample number.

Pearson correlation between pooled strontium values (all groups that received strontium) in serum and bone for each age group did not show any significant linear relationship. The same results were obtained for barium-dosed groups. This indicates that though higher dosage of barium and strontium results in higher serum concentration (until reaching a plateau), this does not necessarily mean that more barium and strontium atoms will incorporate in the bone. It is stipulated that the rate of bone turnover and range of active turnover regions during the administration play a larger role than sole bioavailability in the uptake of elements by bone.

Analysis of raw calcium concentrations in bone or serum showed no statistical difference among treatment groups or age groups. However, analysis of calcium/(gram bone) showed that younger animals had significantly higher calcium/(gram bone) than older animals (1.3-fold difference, $p = 0.001$) (data not shown here). Pearson correlation did not show any significant relation between serum calcium and calcium in bone, whether raw calcium or calcium/bone ratio were used. Element/bone ratio in statistical tests was not used for barium or strontium because of highly site-specific nature of their distributions in bone.

To assess nephrotoxicity of barium and strontium on kidneys urea levels in serum were measured. For statistical analysis, two-way mixed analysis of variance (ANOVA) was used to investigate the interaction of age with treatments. Box plots were used to identify outliers, where any value

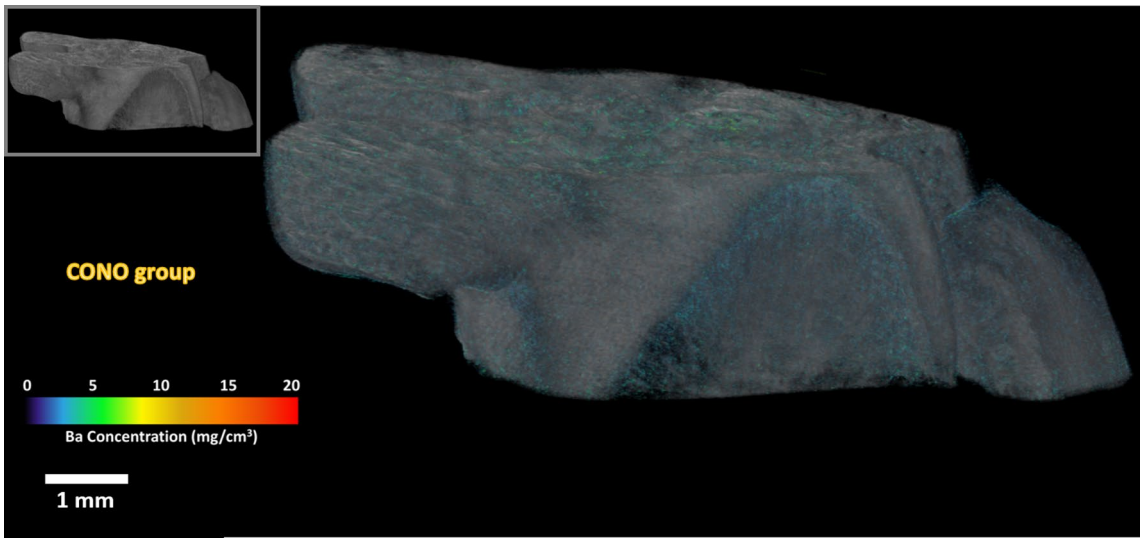

Fig. 4 3D image of the control group. The image shows femur of an adult rat from the control group. The faint signal is likely artifact and created by noise, misregistration, and subtraction of the 'above' and 'below' images. The measured concentration of barium in bone by ICP-MS was negligible. The inset shows a plain 3D model of the respective bone

more than 3 box length was identified as an outlier and hence removed from the analysis. There was a statistically significant two-way interaction between serum urea level and age, in which urea level increased with age, $F(7, 26) = 7.29$, $p < 0.0005$, partial $\eta^2 = 0.662$ (Table 3). For comparison of the mean values, GLM univariate test was used, with Tukey's post hoc test. Treatments did not change urea levels in serum, as evidenced by the lack of difference among groups at week 4. All groups except CONO and BSO showed a significant increase in serum urea levels from week 0 to week 4, which was associated with age (Table 3).

The GLM univariate test and post hoc analysis between groups did not show any significant difference in heart rate or Q–T_c related to treatments in either of the age groups. To investigate the effect of age on cardiovascular parameters, the six treatment groups were divided into two age groups. A two-tailed independent t test indicated that Q–T_c was approximately 8.5 s longer in the older rats ($p = 0.039$) (Table 4). In addition, heart rate was slightly slower in older animals; however, this was not statistically significant.

Discussion

This study showed that barium and strontium, two alkali earth metals, are primarily incorporated in the areas of new bone formation in the skeleton and will co-localize in the same region, where new bone is being formed. It was shown that both adults and juveniles show a similar maximum concentration of barium or strontium per pixel. This is despite the fact that adult rats had more strontium and barium in their bloodstream (as the dosing was based on body weight), and active formation regions are more prevalent in the juvenile animals. The fact that higher levels in the blood did not result in higher levels in the bone reflects that bone turnover rate and extent of calcification area are more relevant than the serum concentration of bone-seeking elements in dictating the amount of element be taken up by bone. As a result, younger individuals or individuals with bone pathologies that alter the rate of remodeling (e.g., blastic bone tumors, osteoporosis, etc.) will accumulate more strontium and barium than healthy adults, but still at the similar maximum concentration per crystal of hydroxyapatite. Li et al. reported that strontium atoms can replace up to 0.5 of 10 calcium atoms in the mineral crystal [5].

KES data for quantifying the concentration of barium in bone are very robust and accurate; however, strontium maps in bone are more likely to suffer from a phenomenon called photon starvation [16]. Because the K-edge energy of strontium is relatively low (16.105 keV) for imaging strontium in such a dense material as bone, the sample must be thin (2–3 mm solid bone); otherwise, attenuation of X-rays will be too great to enable sufficient detection after the sample. In that case, the concentration of strontium is underestimated and the fine details of the image are compromised. Therefore, if the thickness of the sample in XY plane is not less than 2–3 mm of bone, then for quantitative comparison of strontium concentrations in bone, ICP-MS data should be considered as gold standard due to its high precision and low detection limits. Those results correlate well with the EPMA signal strength and indicate that strontium was preferred by bone to barium,

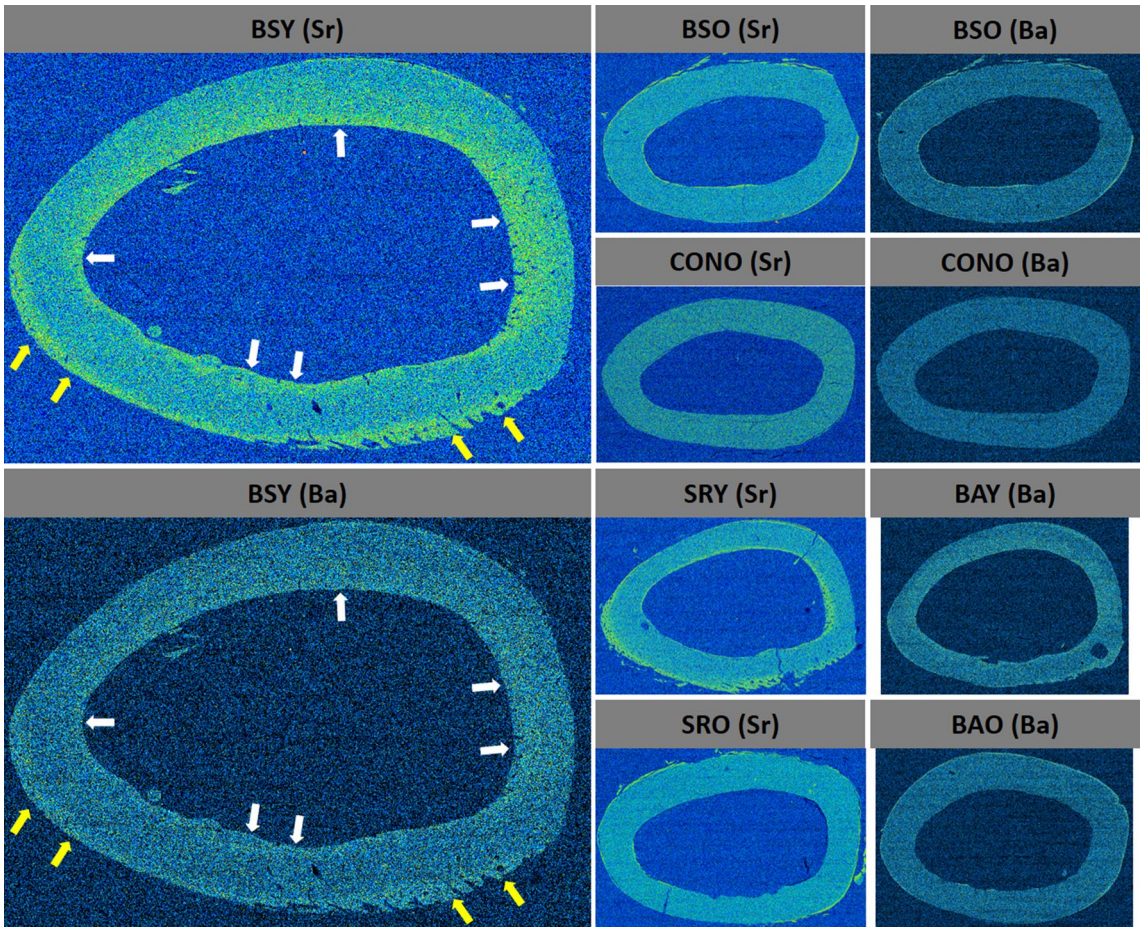

Fig. 5 EPMA 2D cross sections. The panel shows the distribution of barium and strontium (distinguished in parenthesis) in the cortical mid-shaft tibia from various groups. The co-dosed groups (BSY, BSO) show the two elements accumulated in the same regions in each age group. White arrows show incorporation of elements in the endosteum and yellow arrows show deposition in the periosteum layers. No barium and strontium signal was present in the CONO group (i.e., control adults). SRY and BAY images show a similar pattern of deposition in bones of the young rats. SRO and BAO images show the same pattern of deposition for strontium and barium in the adult rats

even though equal molar concentrations, where dosed. Our findings are contrary to what Reeves et al. have suggested that barium uptake by bone is 1.5–5 times higher than calcium and strontium [31]. We discovered that barium actually is deposited in smaller concentrations in bone, but at a faster pace. That is in agreement with the literature [32]. Harrison et al. found that 25 h after I.V. injection of similar radioactivity doses of ^{85}strontium and ^{133}barium into a healthy man, the plasma radioactivity was 19.0 and 1.7% of the initial dose, respectively [32]. Radioactive half-lives of those radionuclides are sufficiently long (65 days and 10 years, respectively) and are not a factor for having less barium in plasma. Barium is cleared from the bloodstream faster than strontium, which also explains the lower barium levels in serum found in our study, since blood collection was performed 24 h after the last dosing. No study has looked at the plasma levels of stable barium chloride and strontium chloride in the same species after oral administration. Oral administration of barium chloride in rats resulted in the highest plasma level at 60 min post-administration [33]. Oral bioavailability of strontium chloride in humans is 25 ± 7% [34]. In rats, only one study has looked at bioavailability of radioactive barium chloride and strontium chloride (following 18 h fasting) after oral administration in which absorption of barium and strontium was 20.0 vs. 24.2% for 6–8-week-old rats and 19.9 vs. 16.7% for 60–70-week-old rats [35]. In this study, we fasted animals for 2 h before and after administration of elements, however, due to the similar chemical structure and charge, we assumed that the bioavailability of barium chloride and strontium chloride is similar. Therefore, we suggest that preference of strontium by bone is likely attributed to the closer ionic radii of Sr^{2+} (132 pm) and Ca^{2+} (114 pm) as opposed to Ba^{2+} radius

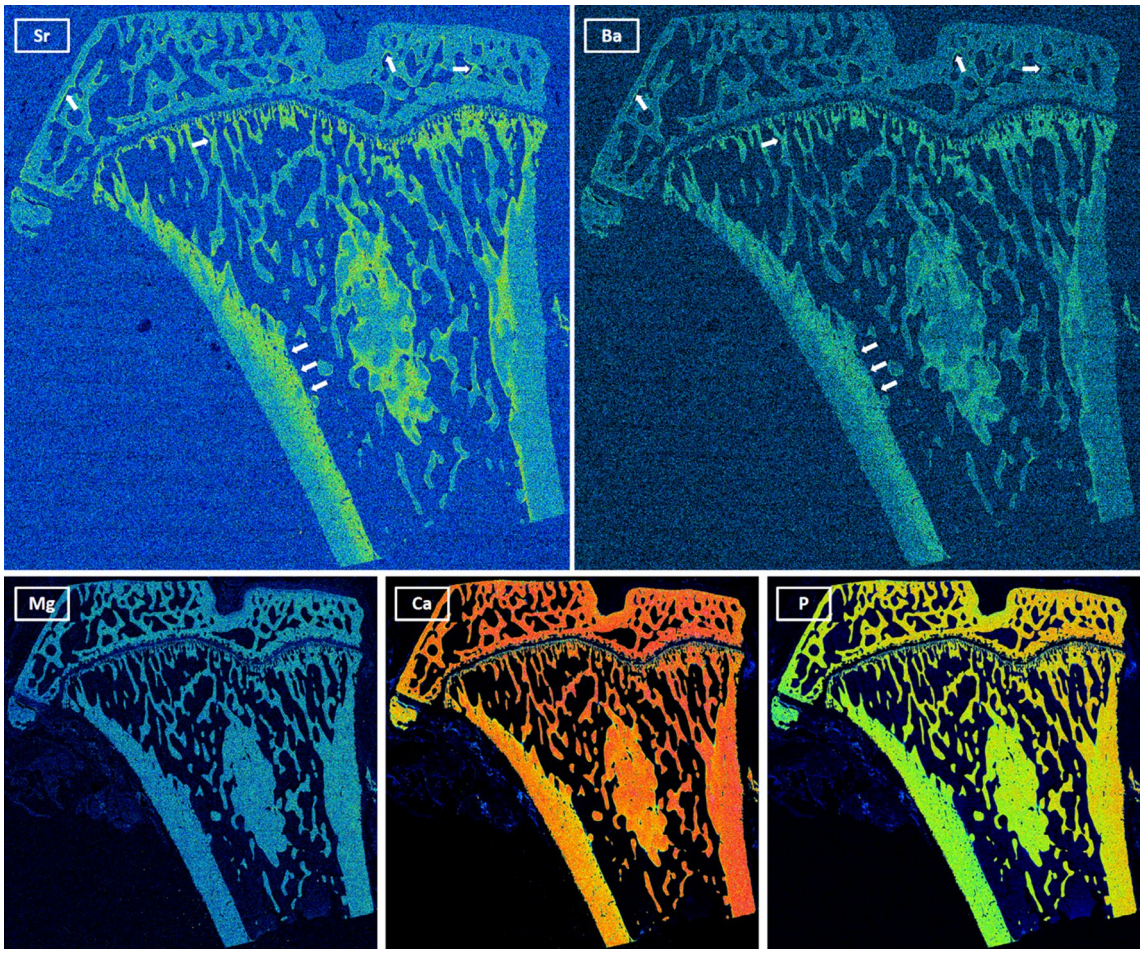

Fig. 6 Elemental distribution in the co-dosed adult rat. The panel represents the distribution of strontium, barium, magnesium, calcium, and phosphorus in the tibia of a co-dosed adult rat. The strontium and barium maps clearly show the incorporation of both elements in the same trabecular and cortical regions (white arrows). The bony region in the diaphyseal marrow shows trabecularization of the cortex (i.e., endosteal bone layer) and is caused by cutting the bone too close to the cortex. It appears that areas that incorporated barium and strontium show slightly less concentration of calcium. That is a logical consequence as a certain number of barium and strontium atoms exchange with calcium atoms in the hydroxyapatite

Table 2 Elemental concentrations in serum and whole tibia

Ca, Ba, and Sr concentrations in serum and whole tibia								
Group	Serum (ng/mL)				Tibia (ppm)			
	Ca	Sr	Ba	*N*	Ca	Sr	Ba	*N*
CONY	102,711 ± 15,497	N/A	0	3	240,111 ± 29,886	N/A	6 ± 1	3
CONO	113,280 ± 5,067	29 ± 18	7 ± 6	3	219,589 ± 12,035	48 ± 2	3 ± 0.3	3
BAY	111,248 ± 3,151	48 ± 8	236 ± 42	3	193,703 ± 44,532	46 ± 7	642 ± 140	3
BAO	110,391 ± 5,008	13 ± 1	259 ± 42	3	223,063 ± 26,321	46 ± 6	244 ± 64	3
BSY	107,706 ± 6,311	908 ± 230	200 ± 51	2	212,573 ± 24,629	1527 ± 186	738 ± 119	3
BSO	108,488 ± 11,553	1,334 ± 400	390 ± 42	3	239,187 ± 15,854	561 ± 89	354 ± 55	3
SRY	105,473 ± 6,221	972 ± 240	4 ± 7	3	169,985 ± 21,338	1,301 ± 570	4 ± 0.5	3
SRO	105,352 ± 4,209	1509 ± 593	0	3	205,828 ± 18,241	640 ± 171	4 ± 2	3

All values are represented as mean ± standard deviation. Concentrations in some samples were below the detection limit of ICP-MS, hence were replaced by 0. The values from the table are represented as graphs in Fig. 7

Fig. 7 Elemental concentration in the serum and whole tibia. Note that concentration of barium and strontium in the serum is higher in the adult rats, though not always statistically significant. This pattern is reversed when the concentrations in the tibiae are considered. In addition, in the co-dosed animals of both ages strontium is preferred to barium by bone even though equal molar concentrations were dosed. For numerical values see table 2.

(149 pm). Ionic radius and electric charge play important roles in the percentage of metals that can replace Ca^{2+} ions in the hydroxyapatite structure.

The toxicological assessments used in this article did not reveal any side effects associated with barium and strontium on the cardiovascular system and kidneys. The increased levels of urea in serum were associated with age and there was no difference among groups [36]. The ECG parameters indicated that *R*–*R* and Q–$T_{c[Fridericia]}$ intervals and heart rates were similar among treatment groups. When animals were pooled according to their ages, it was shown that older animals had approximately 8.5 s longer Q–T_c. The ECG was not collected from control animals; however, since strontium is not a K^+ channel blocker and especially at the sub-therapeutic doses is not known to affect the cardiovascular system adversely, strontium groups were considered as controls for the sake of ECG experiment.

Conclusions

This study for the first time investigated the pattern and extent of incorporation of barium chloride and strontium chloride in the same animals across two age groups in healthy rats. Our results indicated that barium chloride is absorbed from the gastrointestinal tract quicker than strontium chloride and is incorporated in bone faster, however, at smaller concentration. The lack of adverse effects at the low doses administered, and the fact that both elements

Table 3 Serum urea levels (mg/dL)

Group	Baseline		Week 4	
	Mean	*N*	Mean	*N*
CONY	42.2 ± 2.72*	3	63.0 ± 4.03* ($p = 0.005$)	3
CONO	60.5 ± 13.90	3	55.6 ± 1.76 ($p = 0.609$)	3
BAY	43.1 ± 4.80*	5	59.1 ± 0.88* ($p = 0.002$)	5
BAO	50.8 ± 4.62*	5	61.2 ± 7.60* ($p = 0.030$)	5
BSY	44.0 ± 2.90*	5	60.0 ± 3.79* ($p = 0.0005$)	4
BSO	53.8 ± 8.10	5	54.5 ± 8.96 ($p = 0.830$)	5
SRY	41.8 ± 1.47*	4	61.5 ± 2.30* ($p = 0.001$)	5
SRO	49.6 ± 3.80*	5	58.6 ± 3.78* ($p = 0.028$)	5

The urea levels in all treatment groups increased significantly during the 4-week study, except for CONO and BSO. There was no difference in serum urea levels among treatment groups at baseline or endpoint. All values are represented as mean ± standard deviation

*Statistical significance between values of each group from baseline to week 4. For conversion to blood urea nitrogen use: [urea]/2.14

Table 4 ECG parameters

Group	Q–$T_{c[Fridericia]}$ interval (ms)	R–R interval (ms)	Heart rate (ms)	*N*
BAY	91.0 ± 8.6	191.6 ± 13.2	314.5 ± 22.4	5
BAO	96.5 ± 15.5	202.1 ± 15.0	299.2 ± 21.9	5
BSY	86.3 ± 4.4	187.0 ± 18.8	323.6 ± 31.9	4
BSO	93.1 ± 8.7	207.5 ± 21.7	291.9 ± 30.5	4
SRY	84.0 ± 4.4	207.4 ± 23.7	292.3 ± 34.3	4
SRO	94.4 ± 3.3	200.8 ± 9.9	299.5 ± 15.4	4

The Q–T_c was approximately 8.5 s longer in adult rats. There was no difference among treatment groups for the measured parameters

targeted the areas with high calcification rates, comprised of bone formation and/or remodeling, promises that they can be viewed as stable tracers of bone formation and remodeling in preclinical animal models for studying the changes in micro-architecture and bone turnover at high resolution using synchrotron-based imaging such as KES or XRF, or conventional techniques like EPMA and desktop XRF devices. Moreover, barium can also be imaged in vivo utilizing recently introduced spectral KES method [20, 37, 38]. These methodologies promise an exciting fleet of diagnostic and analytic techniques for measuring the efficacy of new pharmaceutical compounds for the treatment of musculoskeletal diseases.

Acknowledgements This study was supported by the Sylvia Fedoruk Canadian Centre for Nuclear Innovation. DMLC and LDC are supported, in part, by the Canada Research Chairs program. AP is a Saskatchewan Health Research Foundation (SHRF) fellow as well as a fellow in the Canadian Institutes of Health Research Training Grant in Health Research Using Synchrotron Techniques (CIHR-THRUST). NS is a CIHR-THRUST fellow. The research described in this paper was performed at the Canadian Light Source, which is supported by the Canada Foundation for Innovation, Natural Sciences and Engineering Research Council of Canada, the University of Saskatchewan, the Government of Saskatchewan, Western Economic Diversification Canada, the National Research Council Canada, and the Canadian Institutes of Health Research.

Author contributions Conception and design: AP and DMLC. Collection and assembly of data: AP and NS. Analysis and interpretation of the data: AP, LDC, LW, and DMLC. Statistical expertise: AP and DMLC. Obtaining of funding: LDC and DMLC. Drafting of the article: AP. Revising manuscript content: AP, LDC, LW, NS, and DMLC. Final approval of the article: AP, LDC, LW, NS, and DMLC. AP and DMLC take responsibility for the integrity of the data analysis.

Compliance with ethical standards

Conflict of interest The authors declare that they have no conflict of interest.

References

1. Pemmer B, Roschger A, Wastl A, Hofstaetter JG, Wobrauschek P, Simon R, Thaler HW, Roschger P, Klaushofer K, Streli C (2013) Spatial distribution of the trace elements zinc, strontium and lead in human bone tissue. Bone 57:184–193. https://doi.org/10.1016/j.bone.2013.07.038
2. Huang J, Zhang TL, Xu SJ, Li RC, Wang K, Zhang J, Xie YN (2006) Effects of lanthanum on composition, crystal size, and lattice structure of femur bone mineral of Wistar rats. Calcif Tissue Int 78:241–247. https://doi.org/10.1007/s00223-005-0294-2
3. Bourgeois D, Burt-Pichat B, Le Goff X, Garrevoet J, Tack P, Falkenberg G, Van Hoorebeke L, Vincze L, Denecke MA, Meyer D, Vidaud C, Boivin G (2015) Micro-distribution of uranium in bone after contamination: new insight into its mechanism of accumulation into bone tissue. Anal Bioanal Chem 407:6619–6625. https://doi.org/10.1007/s00216-015-8835-7
4. Hughes JM, Cameron M, Mariano AN (1991) Rare-earth-element ordering and structural variations in natural rare-earth-bearing apatites. Am Miner 76:1165–1173
5. Li C, Paris O, Siegel S, Roschger P, Paschalis EP, Klaushofer K, Fratzl P (2010) Strontium is incorporated into mineral crystals only in newly formed bone during strontium ranelate treatment. J Bone Miner Res 25:968–975. https://doi.org/10.1359/jbmr.091038
6. Ellsasser JC, Farnham JE, Marshall JH (1969) Comparative kinetics and autoradiography of 45Ca and 133Ba in ten-year-old beagle dogs. The diffuse component distribution throughout the skeleton. J Bone Joint Surg Am 51:1397–1412
7. Fuster D, Herranz D, Vidal-Sicart S, Munoz M, Conill C, Mateos JJ, Martin F, Pons F (2000) Usefulness of strontium-89 for bone pain palliation in metastatic breast cancer patients. Nucl Med Commun 21:623–626
8. Zenda S, Nakagami Y, Toshima M, Arahira S, Kawashima M, Matsumoto Y, Kinoshita H, Satake M, Akimoto T (2013) Strontium-89 (Sr-89) chloride in the treatment of various cancer patients with multiple bone metastases. Int J Clin Oncol. https://doi.org/10.1007/s10147-013-0597-7
9. Seeman E, Boonen S, Borgstrom F, Vellas B, Aquino JP, Semler J, Benhamou CL, Kaufman JM, Reginster JY (2010) Five years treatment with strontium ranelate reduces vertebral and

nonvertebral fractures and increases the number and quality of remaining life-years in women over 80 years of age. Bone 46:1038–1042. https://doi.org/10.1016/j.bone.2009.12.006
10. Reginster JY, Seeman E, De Vernejoul MC, Adami S, Compston J, Phenekos C, Devogelaer JP, Curiel MD, Sawicki A, Goemaere S, Sorensen OH, Felsenberg D, Meunier PJ (2005) Strontium ranelate reduces the risk of nonvertebral fractures in postmenopausal women with osteoporosis: Treatment of Peripheral Osteoporosis (TROPOS) study. J Clin Endocrinol Metab 90:2816–2822. https://doi.org/10.1210/jc.2004-1774
11. Weekes DM, Cawthray JF, Rieder M, Syeda J, Ali M, Wasan E, Kostelnik TI, Patrick BO, Panahifar A, Al-Dissi A, Cooper D, Wasan KM, Orvig C (2017) La(iii) biodistribution profiles from intravenous and oral dosing of two lanthanum complexes, La(dpp)3 and La(XT), and evaluation as treatments for bone resorption disorders. Metallomics 9:902–909. https://doi.org/10.1039/c7mt00133a
12. von Rosenberg SJ, Wehr UA (2012) Lanthanum salts improve bone formation in a small animal model of post-menopausal osteoporosis. J Anim Physiol Anim Nutr (Berl) 96:885–894. https://doi.org/10.1111/j.1439-0396.2012.01326.x
13. Blake GM, Fogelman I (2007) The correction of BMD measurements for bone strontium content. J Clin Densitom 10:259–265
14. Panahifar A, Cooper DM, Doschak MR (2015) 3-D localization of non-radioactive strontium in osteoarthritic bone: role in the dynamic labeling of bone pathological changes. J Orthop Res 33:1655–1662. https://doi.org/10.1002/jor.22937
15. Panahifar A, Swanston TM, Pushie JM, Belev G, Chapman D, Weber L, Cooper DM (2016) Three-dimensional labeling of newly formed bone using synchrotron radiation barium K-edge subtraction imaging. Phys Med Biol 61:5077–5088. https://doi.org/10.1088/0031-9155/61/13/5077
16. Cooper DM, Chapman LD, Carter Y, Wu Y, Panahifar A, Britz HM, Bewer B, Zhouping W, Duke MJ, Doschak M (2012) Three dimensional mapping of strontium in bone by dual energy K-edge subtraction imaging. Phys Med Biol 57:5777–5786. https://doi.org/10.1088/0031-9155/57/18/5777
17. Panahifar A, Maksymowych WP, Doschak MR (2012) Potential mechanism of alendronate inhibition of osteophyte formation in the rat model of post-traumatic osteoarthritis: evaluation of elemental strontium as a molecular tracer of bone formation. Osteoarthritis Cartilage 20:694–702. https://doi.org/10.1016/j.joca.2012.03.021
18. Wu Y, Adeeb SM, Duke MJ, Munoz-Paniagua D, Doschak MR (2013) Compositional and material properties of rat bone after bisphosphonate and/or Strontium ranelate drug treatment. J Pharm Pharm Sci 16:52–64
19. Thomlinson W, Elleaume H, Porra L, Suortti P (2018) K-edge subtraction synchrotron X-ray imaging in bio-medical research. Physica Medica 49:58–76
20. Panahifar A, Samadi N, Swanston TM, Chapman LD, Cooper DM (2016) Spectral K-edge subtraction imaging of experimental non-radioactive barium uptake in bone. Phys Med 32:1765–1770
21. National Toxicology Program (1994) NTP toxicology and carcinogenesis studies of barium chloride dihydrate (CAS No. 10326-27-9) in F344/N rats and B6C3F1 mice (drinking water studies). Natl Toxicol Program Tech Rep Ser 432:1–285
22. Dietz DD, Elwell MR, Davis WE Jr, Meirhenry EF (1992) Subchronic toxicity of barium chloride dihydrate administered to rats and mice in the drinking water. Fundam Appl Toxicol 19:527–537
23. Borzelleca JF, Condie LW, Egle JL (1988) Short-term toxicity (one-and ten-day gavage) of barium chloride in male and female rats. Int J Toxicol 7:675–685. https://doi.org/10.3109/10915818809019542
24. Chavassieux P, Meunier PJ, Roux JP, Portero-Muzy N, Pierre M, Chapurlat R (2014) Bone histomorphometry of transiliac paired bone biopsies after 6 or 12 months of treatment with oral strontium ranelate in 387 osteoporotic women: randomized comparison to alendronate. J Bone Miner Res 29:618–628. https://doi.org/10.1002/jbmr.2074
25. Fuchs RK, Allen MR, Condon KW, Reinwald S, Miller LM, McClenathan D, Keck B, Phipps RJ, Burr DB (2008) Strontium ranelate does not stimulate bone formation in ovariectomized rats. Osteoporos Int 19:1331–1341. https://doi.org/10.1007/s00198-008-0602-6
26. Bolland MJ, Grey A (2016) Ten years too long: strontium ranelate, cardiac events, and the European Medicines Agency. BMJ 354:i5109. https://doi.org/10.1136/bmj.i5109
27. Lund Rasmussen K, Skytte L, D'imporzano P, Orla Thomsen P, Sovso M, Lier Boldsen J, (2017) On the distribution of trace element concentrations in multiple bone elements in 10 Danish medieval and post-medieval individuals. Am J Phys Anthropol 162:90–102. https://doi.org/10.1002/ajpa.23099
28. Ezzo JA (1994) Putting the "chemistry" back into archaeological bone chemistry analysis: modeling potential paleodietary indicators. J Anthropol Archaeol 13:1–34. https://doi.org/10.1006/jaar.1994.1002
29. Wysokinski TW, Chapman D, Adams G, Renier M, Suortti P, Thomlinson W (2007) Beamlines of the biomedical imaging and therapy facility at the Canadian light source—part 1. Nucl Instrum Methods Phys Res Sect A 582:73–76. https://doi.org/10.1016/j.nima.2007.08.087
30. Weitkamp T, Haas D, Wegrzynek D, Rack A (2011) ANKAphase: software for single-distance phase retrieval from inline X-ray phase-contrast radiographs. J Synchrotron Radiat 18:617–629. https://doi.org/10.1107/S0909049511002895
31. Reeves A (1986) Barium. In: Friberg L, Nordberg G, Vouk V (eds) Handbook of metals, 2nd edn. Elsevier Science Publishers, New York, pp 88–89
32. Harrison GE, Carr TE, Sutton A (1967) Distribution of radioactive calcium, strontium, barium and radium following intravenous injection into a healthy man. Int J Radiat Biol Relat Stud Phys Chem Med 13:235–247
33. McCauley PT, Washington IS (1983) Barium bioavailability as the chloride, sulfate, or carbonate salt in the rat. Drug Chem Toxicol 6:209–217. https://doi.org/10.3109/01480548309016025
34. Sips AJ, van der Vijgh WJ, Barto R, Netelenbos JC (1995) Intestinal strontium absorption: from bioavailability to validation of a simple test representative for intestinal calcium absorption. Clin Chem 41:1446–1450
35. Taylor DM, Bligh PH, Duggan MH (1962) The absorption of calcium, strontium, barium and radium from the gastrointestinal tract of the rat. Biochem J 83:25–29
36. Costa E, Fernandes J, Ribeiro S, Sereno J, Garrido P, Rocha-Pereira P, Coimbra S, Catarino C, Belo L, Bronze-da-Rocha E, Vala H, Alves R, Reis F, Santos-Silva A (2013) Aging is associated with impaired renal function, INF-gamma induced inflammation and with alterations in iron regulatory proteins gene expression. Aging Dis 5:356–365. https://doi.org/10.14366/AD.2014.0500356
37. Zhu Y, Samadi N, Martinson M, Bassey B, Wei Z, Belev G, Chapman D (2014) Spectral K-edge subtraction imaging. Phys Med Biol 59:2485–2503. https://doi.org/10.1088/0031-9155/59/10/2485
38. Deman P, Tan S, Belev G, Samadi N, Martinson M, Chapman D, Ford NL (2017) Respiratory-gated KES imaging of a rat model of acute lung injury at the Canadian Light Source. J Synchrotron Radiat 24:679–685. https://doi.org/10.1107/S160057751700193X

Affiliations

Arash Panahifar[1] · L. Dean Chapman[1,2] · Lynn Weber[3] · Nazanin Samadi[4] · David M. L. Cooper[1]

David M. L. Cooper
dml.cooper@usask.ca

[1] Department of Anatomy and Cell Biology, College of Medicine, University of Saskatchewan, Saskatoon, SK, Canada

[2] Canadian Light Source, Saskatoon, SK, Canada

[3] Department of Veterinary Biomedical Sciences, University of Saskatchewan, Saskatoon, SK, Canada

[4] Department of Physics and Engineering Physics, College of Arts and Science, University of Saskatchewan, Saskatoon, SK, Canada